Environ Sci Pollut Res
DOI 10.1007/s11356-015-5570-8

RESEARCH ARTICLE

Formation of hydroxyl radicals and kinetic study of 2-chlorophenol photocatalytic oxidation using C-doped TiO_2, N-doped TiO_2, and C,N Co-doped TiO_2 under visible light

Jirapat Ananpattarachai[1] · **Supapan Seraphin**[2] · **Puangrat Kajitvichyanukul**[1]

Received: 19 June 2015 / Accepted: 7 October 2015

Abstract This work reports on synthesis, characterization, adsorption ability, formation rate of hydroxyl radicals ($OH^•$), photocatalytic oxidation kinetics, and mineralization ability of C-doped titanium dioxide (TiO_2), N-doped TiO_2, and C,N co-doped TiO_2 prepared by the sol–gel method. X-ray diffraction (XRD), scanning electron microscopy (SEM), transmission electron microscopy (TEM), X-ray photoelectron spectroscopy (XPS), and UV–visible spectroscopy were used to analyze the titania. The rate of formation of $OH^•$ for each type of titania was determined, and the OH-index was calculated. The kinetics of as-synthesized TiO_2 catalysts in photocatalytic oxidation of 2-chlorophenol (2-CP) under visible light irradiation were evaluated. Results revealed that nitrogen was incorporated into the lattice of titania with the structure of O-Ti-N linkages in N-doped TiO_2 and C,N co-doped TiO_2. Carbon was joined to the Ti-O-C bond in the C-doped TiO_2 and C,N co-doped TiO_2. The 2-CP adsorption ability of C,N co-doped TiO_2 and C-doped TiO_2 originated from a layer composed of a complex carbonaceous mixture at the surface of TiO_2. C,N co-doped TiO_2 had highest formation rate of $OH^•$ and photocatalytic activity due to a synergistic effect of carbon and nitrogen co-doping. The order of photocatalytic activity per unit surface area was the same as that of the formation rate of $OH^•$ unit surface area in the following order: C,N co-doped TiO_2 > C-doped TiO_2 > N-doped TiO_2 > undoped TiO_2.

Keywords TiO_2 · Hydroxyl radical · Phenol · Visible light · Photocatalyst · Oxidation

Responsible editor: Santiago V. Luis

Electronic supplementary material The online version of this article (doi:10.1007/s11356-015-5570-8) contains supplementary material, which is available to authorized users.

✉ Puangrat Kajitvichyanukul
puangratk@nu.ac.th; kpuangrat@gmail.com

[1] Center of Excellence on Environmental Research and Innovation, Faculty of Engineering, Naresuan University, Phitsanulok 65000, Thailand

[2] Department of Materials Science and Engineering, University of Arizona, Tucson, AZ 85721, USA

Introduction

Nowadays, the application of photocatalysis as an advanced oxidation technology for the removal of organic contaminants has received much attention. One of the major factors governing the removal efficiency of this process is the physicochemical properties of catalysts (Zhao et al. 2008). Titanium dioxide (TiO_2) is the most widely used photocatalyst due to its high activity, optical properties, chemical stability, and nontoxicity. The band gap energy of TiO_2 corresponds with UV light range (λ<380 nm), and thus only a small portion of the solar spectrum is absorbed by TiO_2. Hence, many recent works have been focused on the development of TiO_2 photocatalyst that is capable of efficient utilization of the visible light, the main part of the solar spectrum. Most of the researchers focused on modifying the optical response in visible light range by decreasing of the energy gap of TiO_2. The most environmentally friendly and efficient approach for this modification is the non-metal-doped process with the utilization of N, F, S, and C as a dopant (Ananpattarachai et al. 2009; Pelaez et al. 2009; Han et al. 2011; Liu et al. 2012).

There are two approaches to obtain the band gap narrowing in N-doped TiO_2. The first method is the mixing of nitrogen 2p states with oxygen 2p states on the top of the valence band at the substitutional lattice (Di Valentin et al. 2007). The second method is the generating of inter-gap states induced by the

Published online: 26 October 2015

formation of NO bond with the π character at interstitial lattice sites (Ananpattarachai et al. 2009). The visible light catalytic activity of S-doped TiO_2 requires the overlap of sulfur 3p states and oxygen *2p* states (Tachikawa et al. 2004). Sulfur can substitute either the oxygen as an anion or the titanium as a cation (Yu et al. 2005). For C-doped TiO_2, carbon atoms prefer to be interstitial and substitutional to Ti atoms under oxygen-rich conditions, whereas they prefer to be substitutional to O under anoxic conditions (Di Valentin et al. 2005). Among all nonmetal-doped TiO_2 materials, N- and C-doped TiO_2 nanomaterials have been reported on their superior photocatalytic activity under visible light irradiation. Doping with N becomes an attractive approach due to its comparable atomic size with oxygen, small ionization energy, and good stability. On the other hand, C-doped TiO_2 exhibits the superb catalytic activity. Hence, doping of two kinds of atoms into TiO_2 has attracted considerable interest since it may result in a higher photocatalytic activity than those doped solely with carbon or nitrogen. Several works have been done in synthesizing this C,N co-doped TiO_2 by several methods such as a hydrothermal method (Pang and Abdullah 2013), microemulsion-hydrothermal process (Cong et al. 2006), and sol–gel method (Chen et al. 2007). Those works have reported the increase of photocatalytic activity of this co-doped material under visible light. However, the photocatalytic activity of C-doped TiO_2, N-doped TiO_2, and C,N co-doped TiO_2 is hardly comparable owing to the difference in preparation methods of these three materials, which contributes to the difference in their catalytic activities. To our knowledge, no report is available for the comparative study of the formation of hydroxyl radicals (OH^*), photocatalytic activity, kinetics, and mineralization ability of three types of TiO_2 (C-doped TiO_2, N-doped TiO_2, and C,N co-doped TiO_2). This information is necessary for the selection of catalyst for the application of advanced oxidation technology.

In this work, C-doped TiO_2, N-doped TiO_2, and C,N co-doped TiO_2 nanoparticles were synthesized by a modified sol–gel method. We hypothesized that such materials have increased photocatalytic performance under visible light. This enhancement is possibly due to the optical response arisen from the band gap narrowing as well as better electron–hole separation owing to the formation of heterojunctions. The characteristics of these three materials obtained via the same preparation methods were compared. X-ray diffraction (XRD), scanning electron microscopy (SEM), transmission electron microscopy (TEM), X-ray photoelectron spectroscopy (XPS), and UV–vis spectroscopy were utilized to obtain intrinsic characteristics of all catalysts. The rate of formation of OH^* was determined, and the OH-index was calculated. The kinetics of as-synthesized TiO_2 catalysts in photocatalytic oxidation of 2-chlorophenol under visible light irradiation were evaluated. 2-Chlorophenol was chosen to be the pollutant model in this work owing to its high toxicity towards humans and aquatic life and its extensive use in many industrial activities. Mineralization ability of three catalysts was evaluated from total organic carbon (TOC) measurement of 2-chlorophenol during irradiation. The photocatalytic mechanisms in degradation of 2-chlorophenol using C-doped TiO_2, N-doped TiO_2, and C,N co-doped TiO_2 nanoparticles were discussed.

Materials and methods

Materials

Titanium tetraisopropoxide (TTiP), 4-aminoantipyrine ($C_{11}H_{13}N_3O$), ammonium chloride (NH_4Cl), ammonium hydroxide (NH_4OH), and potassium ferricyanide ($K_3Fe(CN)_6$) were obtained from Aldrich Chemicals. Ethanol (EtOH), nitric acid (HNO_3), terephthalic acid, sulfuric acid (H_2SO_4), sodium hydroxide (NaOH), and 2-chlorophenol (2-CP) were obtained from Merck Chemicals. Ethanolamine, diethanolamine, and triethanolamine were used as dopants. These chemicals were purchased from Acros Organics. All solutions were prepared using 18 MΩ deionized water (H_2O). All chemicals used in this work were of analytical grade which were used as received.

TiO_2 catalyst synthesis

A modified sol–gel method was used to synthesize undoped TiO_2, C-doped TiO_2, N-doped TiO_2, and C,N co-doped TiO_2. Undoped TiO_2 nanoparticles were prepared by using the chemicals with a mole ratio of 1:20:1:1 for TTiP/EtOH/HNO_3/H_2O. The tetraisopropoxide (TTiP) was dissolved in EtOH as the first portion, and the solution was stirred for 30 min. Then, the second EtOH portion was mixed with the mixture solution of H_2O and HNO_3. After mixing both portion, precipitation has occurred. The homogeneous transparent solution was separated from the mixture and kept under stirring conditions for 30 min at 4 °C. After drying at 100 °C for 90 min, the xerogel powders were formed. These powders were calcined at 500 °C for 30 min in an electric tube furnace in air atmosphere.

For the doped TiO_2, a mole ratio of 1:20:1:1:1 for TTiP/EtOH/HNO_3/H_2O/dopant was used. A series of C-doped TiO_2, N-doped TiO_2, and C,N doped TiO_2 was prepared by changing the types of dopant and the calcination conditions. Ethanolamine was used as a dopant for C-doped TiO_2, and the obtained xerogel powders were calcined at 500 °C in air atmosphere. Diethanolamine and triethanolamine were used as dopants for N-doped TiO_2 and C,N co-doped TiO_2, consequently. In all types of TiO_2 catalyst synthesis, 1 M of dopant was used in each condition. The obtained xerogel powders were calcined at 800 °C in a N_2 atmosphere.

TiO_2 catalyst characterization

All synthesized TiO_2 samples were analyzed by SEM, TEM, XRD, XPS, and UV–vis spectroscopy to obtain intrinsic characteristics. The SEM (a field emission Hitachi S-4500) was operated at 15 kV to examine the morphology all types of TiO_2. The TEM (Hitachi H-8100) were operated at 200 kV to obtain the size, shape, and crystallinity of the TiO_2 nanoparticles. The XRD (Philips X-ray diffractometer) was operated using Cu Kα radiation and a step size of 0.02° in the range of 20–70°. The step time was 1 sec to obtain a good signal-to-noise ratio in the mean reflections of the two main TiO_2 crystalline phases, (1 0 1) anatase (2θ−25.281°) and (1 1 0) rutile (2θ−27.495°). The Scherrer equation was used to obtain the average crystallite size of the anatase according to the using the full-width at half-maximum (FWHM) of the (1 0 1) or (1 1 0) peak.

The UV–vis spectroscopy (PerkinElmer UV/Vis Lambda 35 spectrophotometer) with integrating sphere (Lambda 35 (P/N C6951014)) was employed to get the optical absorption spectra of the TiO_2 samples. The Kubelka–Munk theory was used to convert the diffuse reflectance spectra to the absorbance units. The XPS (Kratos 165 Ultra photoelectron spectrometer) was operated with either an Al Kα or Mg Kα monochromatic source to obtain the spectra. The Brunauer, Emmett, and Teller (BET) surface areas were measured by nitrogen adsorption–desorption isotherms at 77 K with a Quantachrome AUTOSORB-1.

Determination of hydroxyl radicals ($OH^{\cdot}$)

The Hitachi F-4500 fluorescence spectrophotometer was used to determine the formation of $OH^{\cdot}$ generated on the photocatalysts' surface under visible light irradiation. The determination procedure was followed the previous published work (Xiao and Ouyang 2009; Wu et al. 2010). In a first solution, a diluted NaOH aqueous solution with a concentration of 2×10^{-3} M was prepared. A second solution with 0.10 g of photocatalyst in 30 mL of terephthalic acid solution with a concentration of 0.83 g/L or 5×10^{-4} M was poured to the first portion and mixed. A 150-W halogen lamp (Sylvania) was used as a visible light source. The intensity of the incident light inside the photoreactor was measured as 0.75×10^{-5} Einstein s^{-1} by uranil actinometer method (Heidt et al. 1979). The solution containing 1 M sodium nitrite was employed as a UV filter to eliminate light <420 nm. The irradiated solution was filtrated through 0.45-μm membrane filter and analyzed by fluorescence spectrophotometer for the measurement of 2-hydroxyterephthalic acid. This acid can be detected at the wavelength of about 425 nm. The fluorescence intensity was recorded to determine the formation rate of $OH^{\cdot}$.

Photochemical reaction

The batch photoreactor was cylindrical shape with a volume of 1.1 L made from quartz glass (ACE Glass Co. 7841-06; Vineland, NJ). A 150-W halogen lamp (Sylvania) was used as a visible light source. A solution containing 1 M sodium nitrite was used as a UV filter to eliminate light <420 nm (Kamat 1993; Cheng et al. 2004). The 2-CP solution was photocatalytic treated in batch operation mode in an oxygen atmosphere. The solution pH value was kept at 7.0 by adding concentrated sulfuric acid to the 2-CP solution. The temperature maintained at 25±2 °C throughout the experiment. After reaching equilibrium in the dark for 30 min, the light was turned on to start photocatalytic reaction. The solution was fully stirred with a magnetic stirrer to ensure sufficient mixing. Aliquots from photocatalytic reactor were withdrawn during time interval and filtered through a membrane filter (0.1 μm).

The aliquots were subsequently reacted with 4-aminoantipyrine in the presence of potassium ferricyanide at pH 7.9±0.1 to form a colored antipyrine dye. The absorbance of this dye was measured at 510 nm by a UV–vis spectrometer (Lambda 35 PerkinElmer). The reaction was performed for 50 min unless otherwise specified. For mineralization determination, the values of initial and treated total organic carbon were analyzed by TOC analyzer (a Shimadzu 700 TOC ANALYZER 0-1 Analytical) after filtration.

Results and discussion

X-ray diffraction

Phase composition and crystallite size of C-doped TiO_2, N-doped TiO_2, and C,N co-doped TiO_2 were analyzed by X-ray diffraction. Figure 1 shows that the anatase phase was the predominant structure in all synthesized TiO_2 nanoparticles. A major peak corresponding to (1 0 1) reflections of the anatase phase of TiO_2 was apparent at the angle of 25.28°, while the minor peaks appeared at 37.80°, 48.05°, 53.89°, and 55.06°. There is no rutile detected in all TiO_2 samples. The average particle size was estimated by applying the Scherrer formula on the anatase (1 0 1) peak (the highest intensity peak):

$$L = \frac{K\lambda}{\beta\cos\theta} \tag{1}$$

where L is the crystallite size, K is a constant (usually 0.89), λ is the wavelength of the X-ray radiation (0.15418 nm for Cu Kα), β is the line width at the half-maximum height, and θ is the corresponding diffraction angle in degrees.

Estimated crystal sizes and surface areas from BET analysis of undoped TiO_2, C-doped TiO_2, N-doped TiO_2, and C,N

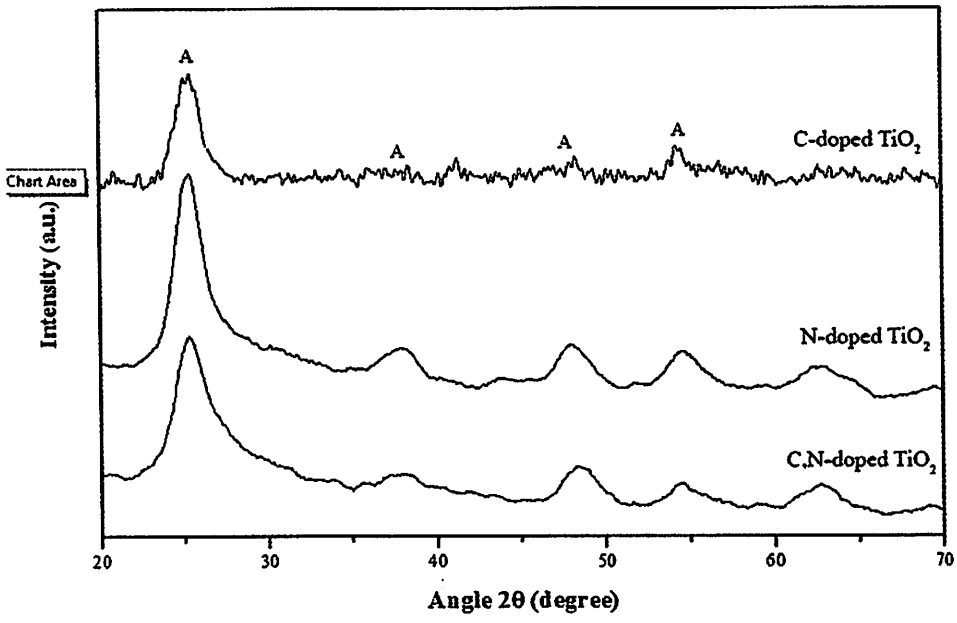

Fig. 1 XRD spectra showing crystal structures of C-, N-, and C,N doped TiO_2

co-doped TiO_2 samples are listed in Table 1. Anatase crystal sizes of three types of TiO_2 were in the range of 5.83–6.87 nm with the surface area in the range of 9.15–12.01 m^2/g. C,N co-doped TiO_2 had the smallest crystal size of the anatase and the highest surface area. However, the corresponding surface area of each titania catalyst was not significantly different.

Morphologies from SEM and TEM

Morphologies of C-doped TiO_2, N-doped TiO_2, and C,N co-doped TiO_2 revealed by SEM micrographs are shown in Fig. 2. All samples appeared as agglomerations of small particles. The TiO_2 nanopowders in all cases presented aggregates consisting of smaller particles (50–100 nm for N-doped TiO_2) to larger particles (about 300–500 nm for C-doped TiO_2) with a high tendency to crystallization. Fine particles with a very homogeneous size distribution can be seen in both N-doped TiO_2 and C,N co-doped TiO_2.

TEM images (Fig. 3) of all three catalysts demonstrated all anatase phase with a uniform dimension with an average crystal size of about 5–8 nm, and no rutile phase was detected. The crystallite sizes observed in the TEM micrographs were consistent with those obtained from the estimation of peak broadening of XRD spectra.

UV–vis spectroscopy and bandgap

The UV–vis spectra of C-doped TiO_2, N-doped TiO_2, C,N co-doped TiO_2, and undoped TiO_2 were shown in Fig. 4. This figure illustrates the response of all synthesized TiO_2 nanopowders to visible light (400–800 nm). Undoped TiO_2 has a higher absorption in UV region (200–300 nm) than the other TiO_2 but no significant absorption in the visible light region. C-doped TiO_2, N-doped TiO_2, and C,N co-doped TiO_2 had high absorption in the visible region but relatively low absorption in UV region compared to undoped TiO_2. This result indicates that the investigated dopants effectively extended absorption of C-doped TiO_2, N-doped TiO_2, and C,N co-doped TiO_2 into the visible light range. This information suggests that visible light absorption ability is mainly dependent on the type of dopant and calcination condition leading to different types of doped TiO_2. Among all types of investigated TiO_2, C,N co-doped TiO_2 provided the highest visible light absorption ability.

The bandgap energy of all synthesized TiO_2 nanopowders can be estimated from plots of the square root of Kubelka–Munk functions $F(R)$ versus photon energy (Asahi et al. 2001). The relation of $(\alpha h\nu)^2$ and $(h\nu)$ was plotted. The bandgap of TiO_2 can be determined from the following equation:

$$ahn = A\left(hn - E_g\right)^r \tag{2}$$

where A is a constant, $h\nu$ is the photon energy, E_g is the optical energy gap of the material, and r is characteristic of the optical transition process, which is equal to 2.0 for an indirect allowed

Table 1 Crystal size and surface area of undoped TiO_2, N-doped TiO_2, C-doped TiO_2, and C,N co-doped TiO_2

TiO_2	Crystal size (nm)	Surface area (m^2/g)
Undoped TiO_2	5.83	12.01
C-doped TiO_2	6.83	9.84
N-doped TiO_2	5.86	11.84
C-N-co-doped TiO_2	6.87	9.15

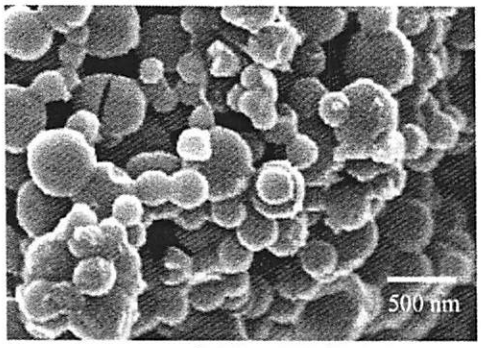

a) C-doped TiO_2

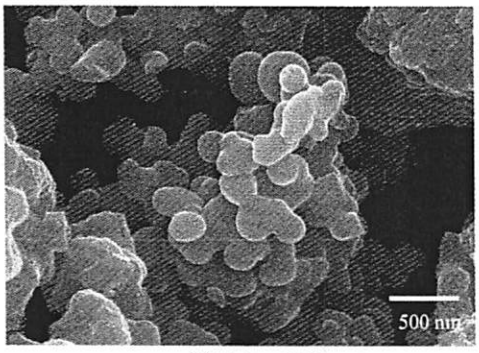

b) N-doped TiO_2

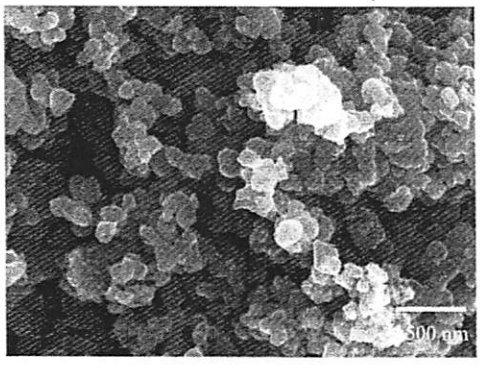

c) C,N-doped TiO_2

Fig. 2 SEM micrographs of **a** C-doped TiO_2, **b** N-doped TiO_2, and **c** C,N doped TiO_2

optical transition of an amorphous semiconductor. Bandgap energies of the investigated TiO_2 nanopowders are summarized in Table 2. Determinations of bandgap for undoped TiO_2 and N-doped TiO_2 are shown in Supplementary Information.

Results show that the bandgap changed from 3.20 eV (undoped TiO_2) to 2.95, 2.85, and 2.80 for C-doped TiO_2, N-doped TiO_2, and C,N co-doped TiO_2, respectively. The value of this bandgap was narrower than the original value. This information reflects the doping effect of carbon and/or nitrogen on the band edges of the TiO_2 and the contribution of carbon and/or nitrogen to the redshift of the bandgap. This narrower bandgap will facilitate excitation of electrons from the valence band to the conduction band in the doped TiO_2 under visible light illumination, which can result in higher photocatalytic activities. The visible light absorption ability of all investigated TiO_2 can be arrayed in the order of C,N co-doped TiO_2 > N-doped TiO_2 > C-doped TiO_2 > undoped TiO_2.

XPS

The high-resolution XPS spectra of N *1s*, C *1s*, Ti *2p*, and O *1s*, taken on the surface of C-doped TiO_2, N-doped TiO_2, and C,N co-doped TiO_2 samples are shown in Fig. 5. The atomic compositions of C, O, Ti, and N elements in each type of TiO_2 were determined as shown in Table 3.

The observed N *1s* spectra were detected in N-doped TiO_2 and C,N co-doped TiO_2, which were in the range of previously reported of nitrogen doping in oxide molecule (Peiró et al. 2001; Sakthivel et al. 2004; Ananpattarachai et al. 2009; Pang and Abdullah 2013). The N *1s* spectrum was detected at 406.1 eV for N-doped TiO_2 and 400.8 and 402.5 eV for C,N co-doped TiO_2 samples. The binding energies of N *1s* spectrum detected in this work were higher than that of the typical binding energy at ≤397.5 eV in Ti-N (Peiró et al. 2001; Sakthivel et al. 2004; Ananpattarachai et al. 2009; Pang and Abdullah 2013). These observed peaks in the range of 398.5–402.5 eV may attribute to the NO species. The main peak at 402.5 eV of C,N co-doped TiO_2 were attributed to NO, indicating the higher concentration of NO in as prepared nitrogen-doped TiO_2 as described in previous work (Peiró et al. 2001). The strong signal at 406.1 eV was reported previously by Sakthivel et al. (2004), and it was assigned to the presence of nitrite specie (NO_2^-). This N *1s* peak may ascribe to electron binding energy of a lower valence state of nitrogen in the environment of O-Ti-N. In addition, the peak localized at 400.8 eV was ascribed to the anionic N^- in O-Ti^{3+}-N linkages in the TiO_2 (Pang and Abdullah 2013). Results from this work suggest that both N-doped TiO_2 and C,N co-doped TiO_2 from investigated nitrogen precursors are interstitial type with different bonding of N and O in the molecular structure of N-doped TiO_2.

The peaks of C *1s* at 284.5 eV were detected in all TiO_2 samples. However, the C *1s* spectrum XPS peaks at 286.5 and 288.6 eV were found in both C-doped TiO_2 and C,N co-doped TiO_2, whereas no appearance of these two peaks was detected in N-doped TiO_2. It was reported previously that the smaller component at a binding energy of 284.5 eV may attribute to C *1s* electrons from the carbon tape (Xiao and Ouyang 2009). The C *1s* peak at 286.5 and 288.6 eV was reported as two types of carbonate species, C–O and C=O, respectively (Papirer et al. 1995). Ohno et al. (2004) observed the carbonate species with binding energies of 288.0 eV in their C-doped TiO_2 samples, and they thought that C^{4+} ions were incorporated into the bulk phase of TiO_2. Ren et al. (2007) also observed that the carbonate species with binding energies of

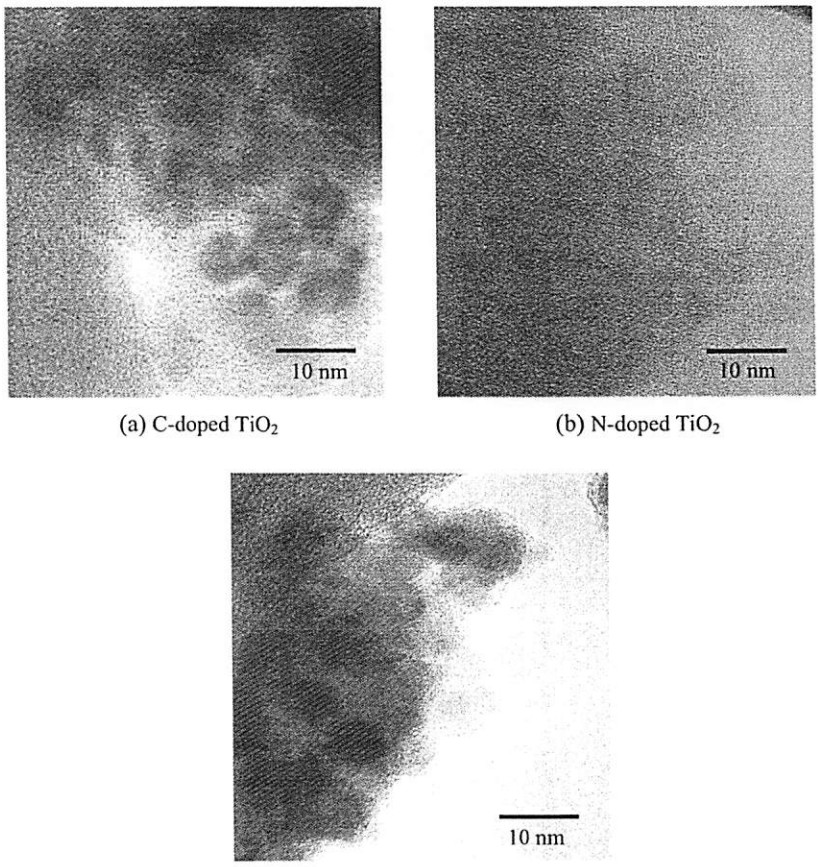

(a) C-doped TiO_2 (b) N-doped TiO_2

(c) C,N –doped TiO2

Fig. 3 TEM micrographs of **a** C-doped TiO_2, **b** N-doped TiO_2, and **c** C,N doped TiO_2

288.6 eV and proposed that carbon may substitute for some of the lattice titanium atoms and form a Ti–O–C structure. Chen et al. (2007) revealed that the doped carbon can form a layer on the surface of TiO_2 nanoparticles with the compound mixture of carbon and carbonate species. This carbonaceous material can increase the absorption ability of TiO_2 for visible light, in the same way, with organic dyes as the photosensitizer during irradiation.

Through deconvolution based on the profile of O *1s*, three peaks were found at 529.6 of C-doped TiO_2 and at 531.3 and 532.4 eV for both N-doped TiO_2 and C,N co-doped TiO_2. The first peak found in C-doped TiO_2 can be assigned to the lattice oxygen in Ti–O bond of TiO_2 (Shao et al. 2008). As described by Sun et al. (2008), the peak at 531.3 eV found in both N-doped TiO_2 and C,N co-doped TiO_2 may arise from $OH^{\bullet}$ radical. The last peak at 532.4 or 534 eV found in both N-doped TiO_2 and C,N co-doped TiO_2 may be contributed to the oxygen of NO_X.

The peaks for Ti $2p_{3/2}$ and Ti $2p_{1/2}$ were located at 458.6 and 464.4 eV for all three types of TiO_2. These binding energies were characteristic of Ti^{4+}. For Degussa P25 (referenced titania), the peaks for Ti $2p_{3/2}$ and Ti $2p_{1/2}$ appeared at 458.9 and 464.7 eV. These peaks were contributed by the linkage of O–Ti–O in TiO_2 (Chen and Burda 2004). Compared with the binding energy of Degussa P25, the binding energy of Ti *2p* of synthesized titania samples decreased after anion doping. Results from this work are in a good agreement with Shao et al. (2008), and it can be explained that the decreasing of binding energy of Ti *2p* is the result from the different electronic interactions of Ti with anions (carbon or nitrogen).

Adsorption ability and isotherm of C-doped TiO_2, N-doped TiO_2, and C,N co-doped TiO_2

Adsorption ability and the adsorption isotherm of three catalysts have been extensively investigated to describe the equilibrium established between adsorbed 2-CP on the TiO_2 as an adsorbent (q_e) and 2-CP remaining in solution (C_e). Preliminary adsorption experiments revealed that, in the absence of TiO_2, there was no noticeable change in 2-CP concentration during 30-min experimental period. The 2-CP adsorption ability of all synthesized TiO_2 was evaluated. The highest concentrations of adsorbed 2-CP on different types of TiO_2 surface were determined. Figure 6 shows that the C, N doped TiO_2 provided the highest adsorption of 2-CP on the surface of titania, whereas undoped TiO_2 provided the lowest

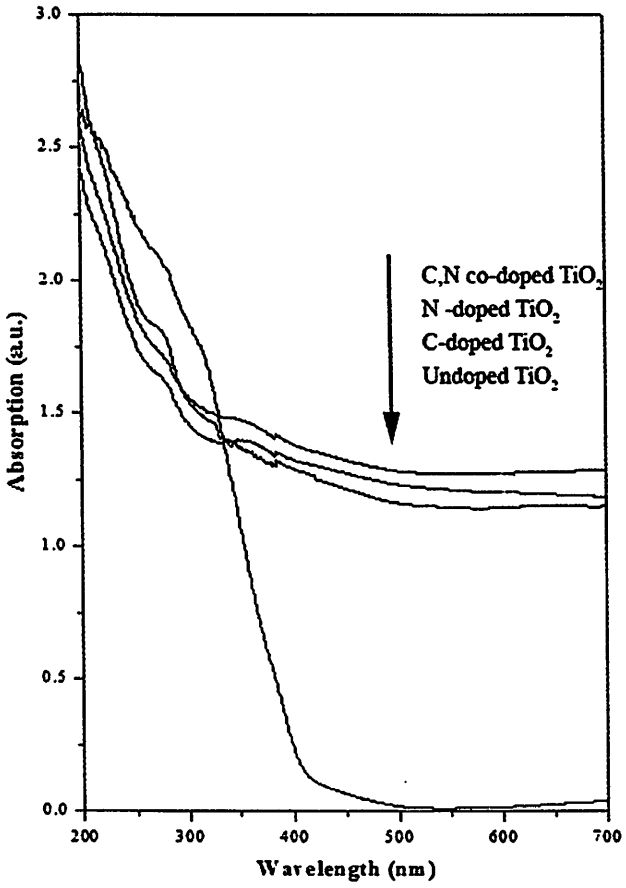

Fig. 4 UV–vis absorption spectra of undoped TiO_2 and C-, N-, and C,N doped TiO_2

adsorption ability. The 2-CP adsorption ability of all investigated TiO_2 can be arrayed in the following order: C,N co-doped TiO_2 > C-doped TiO_2 > N-doped TiO_2 > undoped TiO_2.

Adsorption isotherm of four catalysts, undoped TiO_2, C-doped TiO_2, N-doped TiO_2, and C,N co-doped TiO_2, was conducted using Langmuir and Freundlich models. The Langmuir model assumes a monolayer sorption on a surface and is represented by the following equation:

$$q_e = \frac{q_{max} b C_e}{(1 + bC_e)} \quad (3)$$

where q_{max} is the maximum quantity of 2-CP per unit weight of adsorbent to form a complete monolayer on the surface, C_e is the equilibrium concentration, q_e is the amount of 2-CP adsorbed at equilibrium, and b is the Langmuir constant related to the energy of 2-CP adsorption.

Table 2 Bandgap energy of undoped TiO_2, N-doped TiO_2, C-doped TiO_2, and C,N co-doped TiO_2

TiO_2	Bandgap (eV)
Undoped TiO_2	3.20
C-doped TiO_2	2.95
N-doped TiO_2	2.85
C,N doped TiO_2	2.80

The Freundlich isotherm assumes that the uptake of metal ions occurs on a heterogeneous surface by a multilayer adsorption:

$$q_e = K_f C_e^{(1/n)} \quad (4)$$

where K_f and n are the Freundlich constants related to adsorption capacity and intensity, while C_e and q_e are equilibrium concentrations of adsorbate and the amount adsorbed at equilibrium, respectively.

According to the coefficient correlation (R^2) obtained, Langmuir isotherm of all investigated catalysts had a better fitting model than the Freundlich isotherms because of the higher coefficient correlation. The calculated Langmuir constants for undoped TiO_2, C-doped TiO_2, N-doped TiO_2, and C,N co-doped TiO_2 are summarized in Table 4. The maximum of 2-CP adsorption capacity (q_{max}) on the C,N co-doped TiO_2 (13.889±0.8 mg/g) and C-doped TiO_2 (13.193±0.5 mg/g) was obviously higher than that of N-doped TiO_2 (9.479± 0.8 mg/g) and undoped TiO_2 (5.394±0.4 mg/g). In addition, the b values related to the energy of adsorption for undoped TiO_2, N-doped TiO_2, C-doped TiO_2, and C,N co-doped TiO_2 were 0.095, 0.102, 0.136, and 0.217 L/mg, respectively. It implied that C,N co-doped TiO_2 nanopowders had the highest affinity to adsorb 2-CP among all four catalysts. This finding ascribed that carbonaceous species formed as a layer at the surface of C,N co-doped TiO_2 and C-doped TiO_2 (discussed earlier in XPS analysis) could adsorb more 2-CP than N-doped TiO_2 and undoped TiO_2. This result is in a good agreement with Chen et al. (2007). Moreover, a smallest nanosize of C,N co-doped TiO_2 can provide the highest surface area supporting the highest adsorption ability of 2-CP among all investigated catalysts.

Formation of hydroxyl radicals (OH$^\bullet$) by C-doped TiO_2, N-doped TiO_2, and C,N co-doped TiO_2

Fluorescence technique with terephthalic acid was used to determine the formation of OH$^\bullet$ on the surface of TiO_2 under visible light irradiation. From previous work (Ishibashi et al. 2000; Tryba et al. 2006; Xiao and Ouyang 2009), this terephthalic acid was readily reacted with OH$^\bullet$ to produce highly fluorescent product, 2-hydroxyterephthalic acid. At low concentration of terephthalic acid (less than 10^{-3} M, room temperature), the hydroxylation reaction of terephthalic acid proceeded mainly by OH$^\bullet$. The photogenerated O_2^{-}, $HO_2^\bullet$, and H_2O_2 did not interfere with the reaction between OH$^\bullet$ and terephthalic acid. Hence, the fluorescence intensity attributed to 2-hydroxyterephthalic acid was known to be proportional to the amount of OH$^\bullet$ formed during irradiation

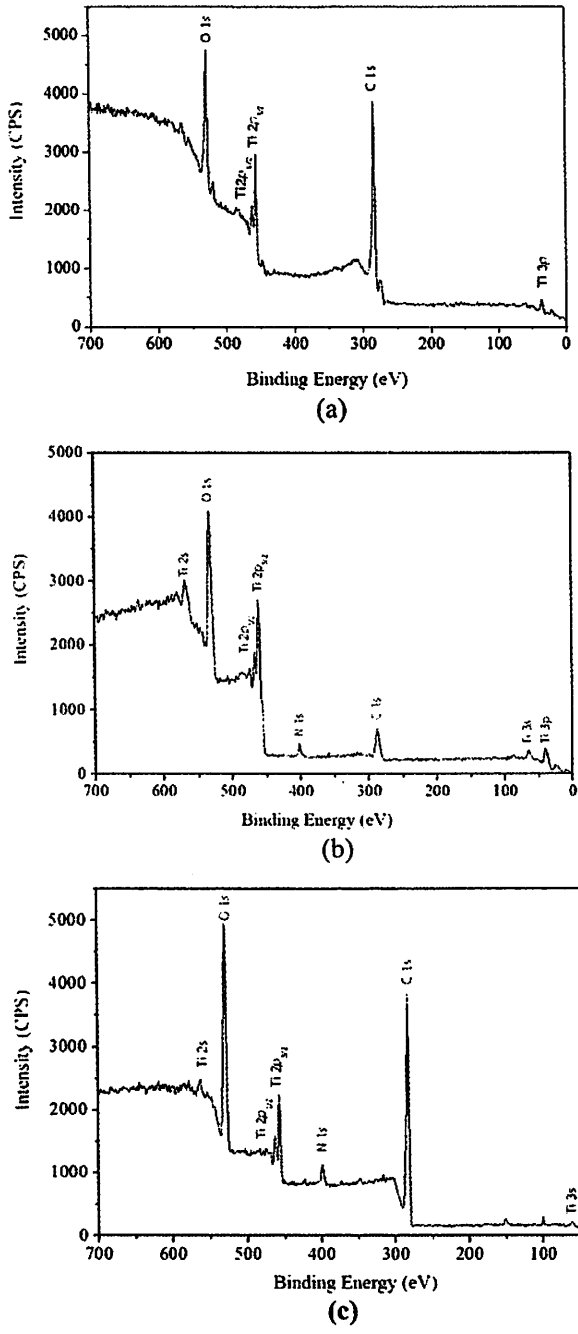

Fig. 5 XPS spectra of a C-doped TiO_2, b N-doped TiO_2, and c C,N doped TiO_2

(Ishibashi et al. 2000; Tryba et al. 2006; Xiao and Ouyang 2009). In addition, the 2-hydroxyterephthalic acid was the only product with any significant fluorescence. In this work, the formation of OH^* by C-doped TiO_2, N-doped TiO_2, and C, N co-doped TiO_2 was determined by following Xiao and Ouyang's work (Xiao and Ouyang 2009).

Figure 7 showed the plots of the r_{OH} per unit surface area using fluorescence spectrophotometer with time for undoped TiO_2, C-doped TiO_2, N-doped TiO_2, and C,N co-doped TiO_2. The rate of OH^* formation or r_{OH} was also calculated from this graph. Results show that OH^* formed at the interface of TiO_2 in all cases were in proportional to the light illumination time obeying zero-order reaction rate kinetics. The formation rate of OH^* could be expressed by the slope of these lines, and the value of formation rate of OH^* (r_{OH}) per units surface area were calculated as shown in Table 5. Recently, Bubacz et al. (2013) introduced a new concept, the "OH-index," to compare the formation rate of OH^* on different photocatalysts. The new parameter referred formation rates of OH^* on the irradiated semiconductor (r_{OH}) to the reference material (r_o). The OH-index was expressed as:

$$\text{OH-index} = \left(r/r_o\right) \times 100 \tag{5}$$

In general, the larger OH-index, the higher photocatalytic activity was observed. Degussa P25 has been used as a material for UV irradiation in Bubacz et al. (2013). Hence, in this work, we also used Degussa P25 as a reference material irradiated under visible light. The OH-index for all investigated catalysts is shown in Table 5.

Table 3 The atomic compositions of C, N, Ti, and O elements in undoped TiO_2, N-doped TiO_2, C-doped TiO_2, and C,N co-doped TiO_2 from XPS analysis

TiO_2	%C content	%N content	%Ti content	%O content
Undoped TiO_2	29.35	0.00	18.21	52.44
C-doped TiO_2	73.93	0.04	7.22	18.81
N-doped TiO_2	26.19	4.11	18.39	51.31
C,N-doped TiO_2	70.63	3.72	2.95	22.70

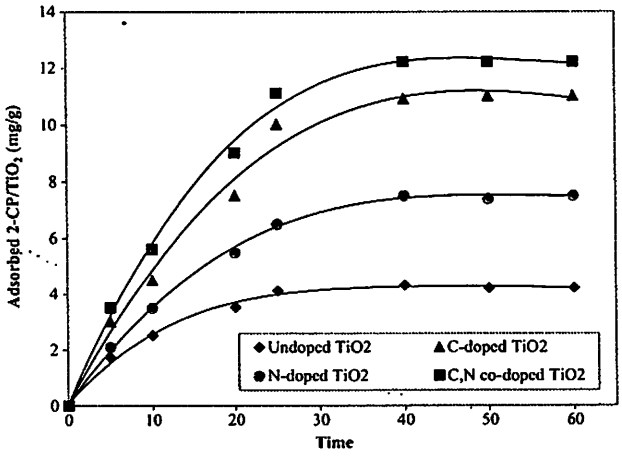

Fig. 6 Adsorption of 2-chlorophenol on the surface of undoped TiO2, C-doped TiO_2, N-doped TiO_2, and C,N co-doped TiO_2. Experimental conditions: $C_{2\text{-CP}}$=50 mg/l, TiO_2=1 g/l

Table 4 Langmuir isotherm and constants of undoped TiO_2, N-doped TiO_2, C-doped TiO_2, and C,N co-doped TiO_2 in 2-CP adsorption process

TiO_2	q_{max} (mg/g)	b (L/mg)	Langmuir equation	R^2
Undoped TiO_2	5.394±0.4	0.095	$q_e=(0.5108C_e)/(1+0.0947C_e)$	0.9616
N-doped TiO_2	9.479±0.5	0.102	$q_e=(0.9631C_e)/(1+0.1016C_e)$	0.9908
C-doped TiO_2	13.193±0.8	0.136	$q_e=(1.7945C_e)/(1+0.136C_e)$	0.9611
C,N-doped TiO_2	13.889±0.8	0.217	$q_e=(3.008C_e)/(1+0.2166C_e)$	0.9847

Results indicate that, during 60-min visible light irradiation on terephthalic acid, C,N co-doped TiO_2 provided the highest value of r_{OH} per unit surface area, whereas Degussa P25 provided the lowest value of r_{OH} per unit surface area. The values of v units surface area of all doped TiO_2 (C-doped TiO_2, N-doped TiO_2, and C,N co-doped TiO_2) were in the range of 14.499–18.130 min^{-1} m^{-2} which were in the same range previously reported for C-doped TiO_2 (Xiao and Ouyang 2009). Both undoped TiO_2 and Degussa P25 exhibited very poor visible light activity r_{OH} due to the bandgap energy of both catalysts was approximately 3 eV. After C and N atoms had been doped into the TiO_2 photocatalysts, the visible light photocatalytic activities of the synthesized samples increased greatly as seen from Fig. 4. The highest formation rate of OH^* for C,N co-doped TiO_2 (v per unit surface area= 18.130 min^{-1} m^{-2}) was five times faster than that of undoped TiO_2 (r_{OH} per unit surface area=3.453 min^{-1} m^{-2}). However, the corresponding formation rate of OH^* for C,N co-doped TiO_2 was slightly higher than that for C-doped TiO_2 (r_{OH} per unit surface area=17.513 min^{-1} m^{-2}) and N-doped TiO_2 (r_{OH} per unit surface area=14.499 min^{-1} m^{-2}). All doping TiO_2 nanopowders also provided a relatively high value of OH-index than undoped TiO_2 and Degussa P25. The nonmetal doping may generate an intermediate energy level above the valence band of TiO_2, thereby narrowing the bandgap to induce visible light absorption (Dong et al. 2008). These results demonstrate that all doping TiO_2 nanopowders (C-doped TiO_2, N-doped TiO_2, and C,N co-doped TiO_2) could be effective visible light-driven and higher activity photocatalysts.

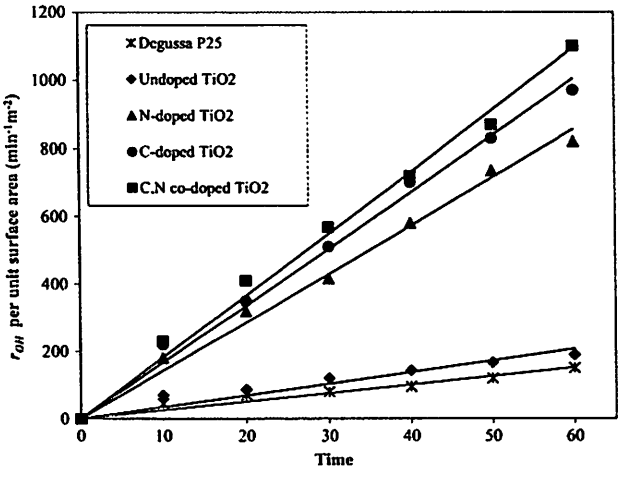

Fig. 7 Plots of the r_{OH} per unit surface area against irradiation time for terephthalic acid (TPA) on Degussa P25, undoped TiO_2, N-doped TiO_2, C-doped TiO_2, and C,N co-doped TiO_2. Experimental conditions: C_{TPA}= 0.83 g/l, TiO_2=3.3 g/l

Visible light irradiation and kinetics of photocatalytic oxidation of 2-chlorophenol

Photocatalytic oxidation of 2-CP by visible light was investigated to obtain photocatalytic activity and kinetic of C-doped TiO_2, N-doped TiO_2, and C,N co-doped TiO_2. The photocatalytic behavior of undoped TiO_2 was also measured as a control. Notably, 2-CP was confirmed to be reasonably photostable in aqueous solution under irradiation by light in the 315–400-nm wavelength range. This chemical undergoes photolysis when irradiated at 254 nm (Ragaini et al. 2001; Bertelli and Selli 2006). In addition, our results in previous work (Ananpattarachai et al. 2009) showed that the 2-CP degradation through direct photolysis in the visible light range was negligible (<4 %). Hence, the 2-CP degradation after treating with all investigated TiO_2 was likely due to the photocatalysis of the applied TiO_2. The photocatalytic reactivity of TiO_2 was represented by the ratio of residual concentration to the initial concentration of 2-CP, C/C_0, as a function of irradiation time in Fig. 8a.

After 90 min irradiation, C,N co-doped TiO_2 has the highest photocatalytic activity under visible light compared with other types of TiO_2. Under the same reaction condition, the photodegradation efficiency of undoped TiO_2 nanoparticles was about 24 %. C-doped TiO_2, N-doped TiO_2, and C,N co-doped TiO_2 all have higher photocatalytic activity than undoped TiO_2. The high performance of the doped TiO_2 tends to be the results of the defects created by the dopants which increased the trapped electrons on the surface of the catalyst. With higher amount of the trapped electrons on the surface of TiO_2, the recombination of the electron–hole pairs is also prevented (Zhang et al. 2014; Shao et al. 2015). These defects also introduced the localized donor energy level under the conduction band, further narrowing the bandgap of the TiO_2 as shown in Table 2.

The photocatalytic activity of C-doped TiO_2 is also greater than that of N-doped TiO_2. The highest photocatalytic activity of the C,N co-doped TiO_2 might have been

Table 5 Formation rate of OH$^{\cdot}$ (r_{OH}) per unit surface area and OH-index of Degussa P25, undoped TiO_2, N-doped TiO_2, C-doped TiO_2, and C,N co-doped TiO_2

TiO_2	r_{OH} (min^{-1})	r_{OH} per unit surface area (min^{-1} m^{-2})	r_{OH}/r_o	OH-index
Degussa P25	2.533	0.461	1.000	100
Undoped TiO_2	3.456	3.453	7.497	625
N-doped TiO_2	14.267	14.499	31.482	3,148
C-doped TiO_2	16.725	17.513	38.027	3,803
C,N-co-doped TiO_2	18.221	18.130	39.367	3,936

due to the existence of a synergistic effect of carbon and nitrogen co-doping. Nitrogen can initiate the intense absorption in the visible light range (Fig. 4) and a redshift in the bandgap transition (Table 2). Hence, more photogenerated electrons and holes participated in the photocatalytic reactions under visible light, and more radicals were produced by the photocatalytic oxidation. Carbon doping introduced a complex mixture of active carbon and carbonate species at the surface of TiO_2 nanoparticles (Sakthivel et al. 2004; Chen et al. 2007). In our photocatalytic process, 2-CP should be preconcentrated and adsorbed on the surface of the TiO_2 nanoparticles led to a higher efficiency in 2-CP degradation during irradiation. Thus, C,N co-doped TiO_2 and C-doped TiO_2 could adsorb 2-CP molecules in a larger amount than N-doped TiO_2 and undoped TiO_2. Besides, the carbonaceous materials formed by doped C atoms act a role of photosensitizer like organic dyes (Chen et al. 2007). These carbons could be excited and injected electrons into the conduction band of TiO_2 resulted in a higher efficiency of C, N co-doped TiO_2 and C-doped TiO_2 than that of N-doped TiO_2.

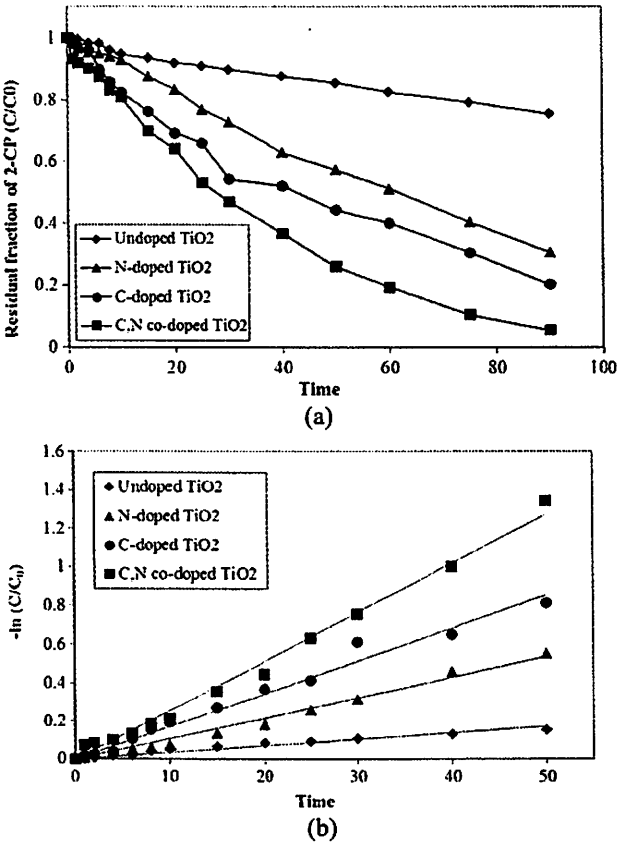

Fig. 8 Photocatalytic oxidation of 2-chlorophenol using different types of TiO_2. a The residual fraction plot and b the $-ln\ (C/C_0)$ versus reaction time and b 2-chlorophenol degradation versus reaction time. Experimental conditions: $C_{2\text{-}CP}$=10–120 mg/l, TiO_2=1 g/l, pH 7

From kinetic studies on photocatalytic reactions of all types of TiO_2, the reaction can be well explained by a pseudo-first-order pattern, with the following equation demonstrating the relationship of C and t:

$$\ln\left(\frac{[C]}{[C]_0}\right) = -k_{obs}t \tag{6}$$

where k_{obs} is the apparent reaction rate constant, t the reaction time, C_0 the initial concentration of 2-CP in aqueous solution, and C the residual concentration of 2-CP at time t. The value of k_{obs} was determined from the slope of the graph plotted between $-ln\ (C/C_0)$ and the reaction time (Fig. 8b). The R^2 value for linear regression was calculated to exhibit the tendency of the reaction, which followed the pseudo-first-order pattern. Values of the initial rate, r, kinetic constant, k_{obs}, and the half-life of 2-CP, $t_{1/2}$, calculated from the pseudo-first-order equations are shown in Table 6.

Results show that within 50 min of visible light irradiation in the presence of the doped TiO_2 catalysts, the degradation rate of 2-CP was 0.2696, 0.9944, 1.2978, and 1.7155 mg/L-min for undoped TiO_2, N-doped TiO_2, C-doped TiO_2, and C,N co-doped TiO_2, respectively. This pattern suggests that the reaction rate can be enhanced by nitrogen and/or carbon incorporation into the TiO_2 matrix. The reaction rate enhancement of the C,N co-doped TiO_2 was sixfold higher than that of the undoped TiO_2. The rate constant of the undoped TiO_2 reaction was only 0.35×10^{-2} min^{-1}, whereas the rate constant of the C,N co-doped TiO_2 was 2.55×10^{-2} min^{-1}. This increase may have been attributable to the synergistic effect of carbon and nitrogen doping as discussed previously.

Table 6 Values of kinetic parameters included initial rate, r, kinetic constant, k_{obs}, and half-lives of 2-chlorophenol, $t_{1/2}$, from the photocatalytic reactions of undoped TiO_2, N-doped TiO_2, C-doped TiO_2, and C,N co-doped TiO_2

TiO_2	r (mg/L min)	k (min^{-1})	$t_{1/2}$ (min)	%Removal
Undoped TiO_2	0.2696	0.0035	198.0421	24.53
N-doped TiO_2	0.9944	0.0107	64.78011	69.36
C-doped TiO_2	1.2978	0.0171	40.53492	79.74
C,N doped TiO_2	1.7155	0.0255	27.18224	94.39

Mineralization of 2-chlorophenol using C-doped TiO_2, N-doped TiO_2, and C,N co-doped TiO_2 under visible light

The degradation percentage of 2-CP in terms of mineralization of TOC in the presence of undoped TiO_2, C-doped TiO_2, N-doped TiO_2, and C,N co-doped TiO_2 was also investigated. The initial concentration of 2-CP was 100 mg/L with an initial TOC value of 80 mg/L. The degradation percentage and mineralization to total organic carbon of 2-CP in the presence of the four types of doped TiO_2 catalysts are shown in Fig. 9. In all cases, rapid degradation of phenol occurred and the 2-CP concentration decreased after irradiation for 30 min. Mineralization of 2-CP in the presence of undoped TiO_2 showed the lowest yield. Results indicate that C,N co-doped TiO_2 provided the lowest residual concentration of TOC for 2-CP. Other types of C-doped TiO_2 and N-doped TiO_2 can reduce TOC concentration, as well. The mineralization ability of all doped TiO_2 catalysts and 2-CP degradation performance can be ranked in the following order: C,N co-doped TiO_2 > C-doped TiO_2 > N-doped TiO_2 > undoped TiO_2.

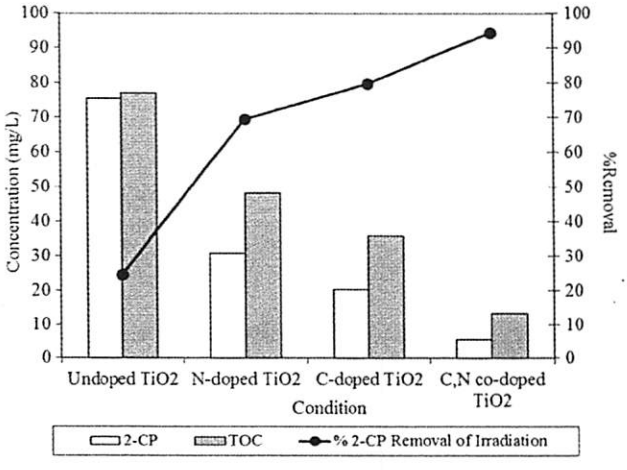

Fig. 9 Percentage removal of total organic carbon (TOC) of 2-chlorophenol in the presence of undoped TiO_2, C-doped TiO_2, N-doped TiO_2, and C,N co-doped TiO_2. Experimental conditions: $C_{2\text{-}CP}$=100 mg/l, C_{TOC}=80 mg/l, TiO_2=1 g/l, pH 7

From photocatalytic activity and mineralization ability in 2-CP degradation, the possible mechanism to generate active species of C,N co-doped TiO_2 could be explained in Fig. 10.

In C-doped TiO_2, carbon doping can improve the adsorption of 2-CP from a complex mixture of active carbon and carbonate species at the surface of TiO_2 nanoparticles. Thus, 2-CP adsorbed on the carbonaceous layer can transfer to the residual vacancies through surface diffusion, which may be a faster process than free diffusion in solution. Moreover, the carbonaceous specie (C) formed by doped C atoms acts a role of photosensitizer (C*) like organic dyes (Chen et al. 2007). This carbonaceous specie can be excited and inject electrons into the conduction band of TiO_2. Thus, these electrons (e^-) could be transferred to oxygen (O_2) absorbed on the TiO_2 surface, which can further transform to H_2O_2 and $OH^\bullet$, resulting in the oxidation of 2-CP.

For N-doped TiO_2, nitrogen doping can lead the redshift of the bandgap that can facilitate excitation of electrons from the valence band to the conduction band in the doped TiO_2 under visible light illumination (Ananpattarachai et al. 2009). Nitrogen doping can create intra-bandgap states (IB) close to the valence band edges, which induces visible light absorption at the new formation bandgap (Chen et al. 2007). The intercalated nitrogen can also shift the position of flat-band (FB) potential to a higher level than that of undoped TiO_2.

Those major effects of carbon and nitrogen are the synergistic effect of C,N co-doped TiO_2 in 2-CP degradation, and the overall reactions during irradiation are shown below.

$$TiO_2 + hv \rightarrow e^- + h^+ \quad (7)$$

$$C + hv \rightarrow C^* + e^- \quad (8)$$

$$Ti^{4+} + e^- \rightarrow Ti^{3+} \quad (9)$$

$$O_{2surf} + e^- \rightarrow O_2^{\bullet-} \quad (10)$$

$$O_2^{\bullet-} + H^+ \rightarrow HOO^\bullet \quad (11)$$

$$2HOO^\bullet + H_2O \rightarrow H_2O_2 + OH^\bullet \quad (12)$$

$$H_2O_2 + hv \rightarrow 2OH^\bullet \quad (13)$$

$$h^+ + 2\text{-}CP \rightarrow \text{Degraded products} \quad (14)$$

$$OH^\bullet + 2\text{-}CP \rightarrow \text{Degraded products} \quad (15)$$

The 2-CP was initially adsorbed by carbonaceous species (C) on the surface of C,N co-doped TiO_2. Under visible light irradiation, both electrons (e^-) from the IB valence band of TiO_2 (Eq. 7) and the carbonaceous species were generated (Eq. 8). The electrons from the intra-bandgap states above the valence band were energetically captured at the new FB potential of the conduction band, then further transferred, and localized to the lower energy level below the conduction band (Eq. 9) (Yang et al. 2006). This Ti^{3+} state was known to be the most reactive site for the oxidation process on TiO_2 surface (Suriye et al. 2007). Electrons from this state reacted with the

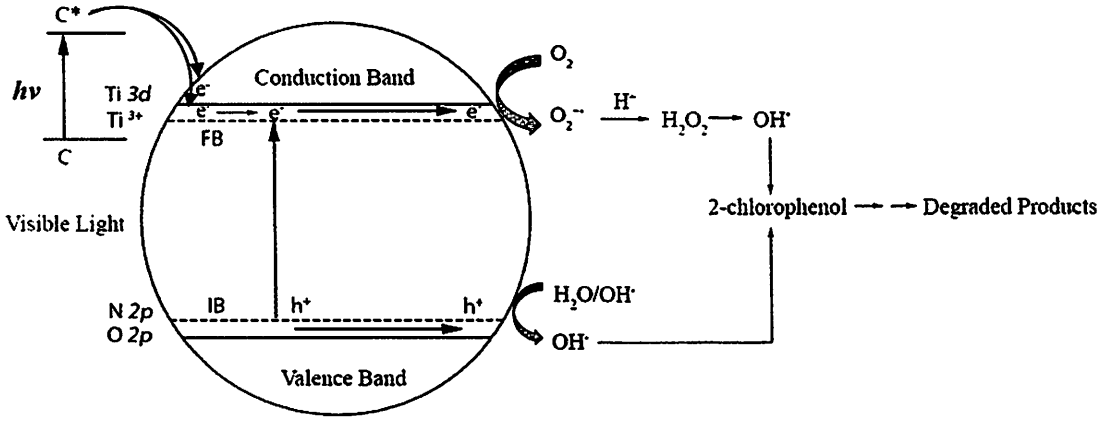

Fig. 10 Schematic of tentative mechanism for 2-chlorophenol degradation on C,N co-doped TiO_2 under visible light

surface-adsorbed oxygen molecules (O_{2surf}), and the superoxide anion radicals ($O_2^{\cdot-}$) were obtained (Eq. 10). These radicals can further transform to H_2O_2 and $OH^{\cdot}$ (Eqs. 11–13), resulting in the oxidation of 2-CP adsorbed on the surface of C,N co-doped TiO_2. In the meantime, the generated electrons from the carbonaceous species can be injected into the conduction band of TiO_2 for further oxidation reaction of 2-CP. Thus, the rate of electron transfer in 2-CP degradation was enhanced. The direct oxidation of 2-CP by generated holes (h^+) from the new IB states also occurred. The generated holes can either directly oxidize 2-CP adsorbed on C,N co-doped TiO_2 surface (Eq. 14) or degrade indirectly through $OH^{\cdot}$ generated by the reaction of holes and water molecules (Eq. 15). Hence, with the co-doping of carbon and nitrogen in the lattice of TiO_2 structure, the degradation of 2-CP was enhanced by synergistic effects of both anion species. For the degradation of 2-CP, our detected intermediate product was mainly hydroquinone, and the final products were carbon dioxide, chlorine ion (Cl^-), and water.

Conclusion

C-doped TiO_2, N-doped TiO_2, and C,N co-doped TiO_2 display differences in visible light absorption ability and bandgap energies with different TiO_2 structures. XPS results show that nitrogen was ascribed to interstitial N with the structure of O–Ti–N linkages in N-doped TiO_2 and C,N co-doped TiO_2; carbon was assigned to the Ti–O–C bond in the C-doped TiO_2 and C,N co-doped TiO_2; both carbon and nitrogen were detected in TiO_2 structure of C,N co-doped TiO_2. The higher 2-CP adsorption ability of C,N co-doped TiO_2 and C-doped TiO_2 than other types of TiO_2 due to a layer composed of a complex carbonaceous mixture at the surface of TiO_2. C,N co-doped TiO_2 nanopowders had higher formation rate of $OH^{\cdot}$ and photocatalytic activity than those doped solely with carbon or nitrogen under visible light. The order of photocatalytic activity per unit surface area was the same as that of the formation rate of $OH^{\cdot}$ unit surface area, which can be ranked in the following order: C,N co-doped TiO_2 > C-doped TiO_2 > N-doped TiO_2 > undoped TiO_2. The highest performance in 2-CP degradation of C,N co-doped TiO_2 was accounted for a synergistic effect of carbon and nitrogen co-doping. C atoms act a role of photosensitizer that can be excited and inject electrons into the conduction band of TiO_2. Thus, these electrons (e^-) could be transfer to oxygen (O_2) absorbed on the TiO_2 surface, which can further transform to H_2O_2 and $OH^{\cdot}$, resulting in the oxidation of 2-CP. Nitrogen atoms induced the new IB states close to the valence band and shift the position of FB potential to a higher level than that of undoped TiO_2. This study on the C-doped TiO_2, N-doped TiO_2, and C,N co-doped TiO_2 not only provides fundamental data for the properties of those doping TiO_2 nanoparticles but also provides in-depth data in formation rate of $OH^{\cdot}$, photocatalytic oxidation kinetics and mineralization ability of these materials in environmental applications, specifically for the treatment of 2-CP-contaminated water.

Acknowledgments This research was supported by Naresuan University Research (No. R2558B045) through Center of Excellence on Environmental Research and Innovation, Faculty of Engineering, Naresuan University.

References

Ananpattarachai J, Kajitvichyanukul P, Seraphin S (2009) Visible light absorption ability and photocatalytic oxidation activity of various interstitial N-doped TiO_2 prepared from different nitrogen dopants. J Hazard Mater 168:253–261. doi:10.1016/j.jhazmat.2009.02.036

Asahi R, Morikawa T, Ohwaki T, Aoki A, Yaga Y (2001) Visible-light photocatalysis in nitrogen-doped titanium oxides. Science 293:269–271. doi:10.1126/science.1061051

Bertelli M, Selli E (2006) Reaction paths and efficiency of photocatalysis on TiO_2 and of H_2O_2 photolysis in the degradation of 2-chlorophenol. J Hazard Mater 138:46–52. doi:10.1016/j.jhazmat.2006.05.030

Bubacz K, Kusiak-Nejman E, Tryba B, Morawski AW (2013) Investigation of OH radicals formation on the surface of TiO_2/N photocatalyst at the presence of terephthalic acid solution. Estimation of optimal conditions. J Photochem Photobiol A 261: 7–11. doi:10.1016/j.jphotochem.2013.04.003

Chen X, Burda C (2004) Photoelectron spectroscopic investigation of nitrogen-doped titania nanoparticles. J Phys Chem B 108:15446–15449. doi:10.1021/jp0469160

Chen D, Jiang Z, Geng J, Wang Q, Yang D (2007) Carbon and nitrogen co-doped TiO_2 with enhanced visible-light photocatalytic activity. Ind Eng Chem Res 46:2741–2746. doi:10.1021/ie061491k

Cheng P, Li W, Zhou T, Jin Y, Gu M (2004) Physical and photocatalytic properties of zinc ferrite doped titania under visible light irradiation. J Photochem Photobiol A 168:97–101

Cong Y, Chen F, Zhang J, Anpo M (2006) Carbon and nitrogen-codoped TiO_2 with high visible light photocatalytic activity. Chem Lett 35: 800–801

Di Valentin C, Pacchioni G, Selloni A (2005) Theory of carbon doping of titanium dioxide. Chem Mater 17:6656–6665

Di Valentin C, Finazzi E, Pacchioni G, Selloni A, Livraghi S, Paganini MC, Giamello E (2007) N-doped TiO_2: theory and experiment. Chem Phys 339:44–56

Dong F, Zhao W, Wu Z (2008) Characterization and photocatalytic activities of C, N and S co-doped TiO_2 with 1D nanostructure prepared by the nano-confinement effect. Nanotechnology 19(365607):1–10

Han C, Pelaez M, Likodimos V, Kontos AG, Falaras P, O'Shea K, Dionysiou DD (2011) Innovative visible light-activated sulfur doped TiO_2 films for water treatment. Appl Catal B 107:77–87

Heidt LJ, Tregay GW, Middleton FA (1979) Influence of the pH upon the photolysis of the uranyl oxalate actinometer system. J Phys Chem 74:1876–1882

Ishibashi K, Fujishima A, Watanabe T, Hashimoto K (2000) Detection of active oxidative species in TiO_2 photocatalysis using the fluorescence technique. Electrochem Commun 2:207–210

Kamat PV (1993) In: Ollis DF, Al-Ekabi H (eds) Photocatalytic purification and treatment of water and air. Elsevier Science Publishers BV, Amsterdam, pp 455–500

Liu GL, Han C, Pelaez M, Zhu DW, Liao SJ, Likodimos V, Ioannidis N, Kontos AG, Falaras P, Dunlop PSM, Byrne JA, Dionysiou DD (2012) Synthesis, characterization and photocatalytic evaluation of visible light activated C-doped TiO_2 nanoparticles. Nanotechnology 23:294003

Ohno T, Tsubota T, Toyofuku M, Inaba R (2004) Photocatalytic activity of a TiO_2 photocatalyst doped with C^{4+} and S^{4+} ions having a rutile phase under visible light. Catal Lett 98:255–258

Pang YL, Abdullah AZ (2013) Effect of carbon and nitrogen co-doping on characteristics and sonocatalytic activity of TiO_2 nanotubes catalyst for degradation of Rhodamine B in water. Chem Eng J 214: 129–138

Papirer E, Lacroix R, Donnet J-B, Nanse G, Fioux P (1995) XPS study of the halogenation of carbon black—part 2. Chlorination. Carbon 33: 63–72

Peiró AM, Ayllón JA, Peral J, Doménech X (2001) TiO_2-photocatalyzed degradation of phenol and ortho-substituted phenolic compounds. Appl Catal B 30:359–373

Pelaez M, de la Cruz AA, Stathatos E, Falaras P, Dionysiou DD (2009) Visible light-activated NF-codoped TiO_2 nanoparticles for the photocatalytic degradation of microcystin-LR in water. Catal Today 144:19–25

Ragaini V, Selli E, Bianchi CL, Pirola C (2001) Sono-photocatalytic degradation of 2-chlorophenol in water: kinetic and energetic comparison with other techniques. Ultrason Sonochem 8:251–258

Ren W, Ai Z, Jia F, Zhang L, Fan X, Zou Z (2007) Low temperature preparation and visible light photocatalytic activity of mesoporous carbon-doped crystalline TiO_2. Appl Catal B 69:138–144

Sakthivel S, Janczarek M, Kisch H (2004) Visible light activity and photoelectrochemical properties of nitrogen-doped TiO_2. J Phys Chem B 108:19384–19387

Shao G-S, Zhang X-J, Yuan Z-Y (2008) Preparation and photocatalytic activity of hierarchically mesoporous-macroporous $TiO_{2-x}N_x$. Appl Catal B 82:208–218

Shao P, Tian J, Zhao Z, Shi W, Gao S, Cui F (2015) Amorphous TiO_2 doped with carbon for visible light photodegradation of rhodamine B and 4-chlorophenol. Appl Surf Sci 324:35–43

Sun H, Bai Y, Jin W, Xu N (2008) Visible-light-driven TiO_2 catalysts doped with low-concentration nitrogen species. Sol Energy Mater Sol Cells 92:76–83

Suriye K, Praserthdam P, Jongsomjit B (2007) Control of Ti^{3+} surface defect on TiO_2 nanocrystal using various calcination atmospheres as the first step for surface defect creation and its application in photocatalysis. Appl Surf Sci 253:3849–3855

Tachikawa T, Tojo S, Kawai K, Endo M, Fujitsuka M, Ohno T, Nishijima K, Miyamoto Z, Majima T (2004) Photocatalytic oxidation reactivity of holes in the sulfur- and carbon-doped TiO_2 powders studied by time-resolved diffuse reflectance spectroscopy. J Phys Chem B 108: 19299–19306

Tryba B, Morawski AW, Inagaki M, Toyota M (2006) The kinetic of phenol decomposition under UV irradiation with and without H_2O_2 on TiO_2, Fe–TiO_2 and Fe–C–TiO_2 photocatalysts. Appl Catal B 63:215–221

Wu Y, Xing M, Zhang J, Chen F (2010) Effective visible light-active boron and carbon modified TiO_2 photocatalyst for degradation of organic pollutant. Appl Catal B 97:182–189

Xiao Q, Ouyang L (2009) Photocatalytic activity and hydroxyl radical formation of carbon-doped TiO_2 nanocrystalline: effect of calcination temperature. Chem Eng J 148:248–253

Yang J, Bai H, Tan X, Lian J (2006) IR and XPS investigation of visible-light photocatalysis-nitrogen–carbon-doped TiO_2 film. Appl Surf Sci 253:1988–1994

Yu JC, Ho WK, Yu JG, Yip H, Wong PK, Zhao JC (2005) Efficient visible-light-induced photocatalytic disinfection on sulfur-doped nanocrystalline titania. Environ Sci Technol 39: 1175–1179

Zhang X, Qin J, Xue Y, Yu P, Zhang B, Wang L, Liu R (2014) Effect of aspect ratio and surface defects on the photocatalytic activity of ZnO nanorods. Nat Sci Rep 4:4596

Zhao ZY, Liu QJ, Zhu ZHQ (2008) Effects of S doping on the electronic structures and photocatalytic properties of anatase TiO_2. Acta Phys 57:3760–3767